

## Use of Grape Leaves for Producing Graphene for Use as an Oxygen Reduction Electrocatalyst

S. Sadegh Hassani<sup>1,2</sup>, M.R. Ganjali<sup>1,3,\*</sup>, L. Samiee<sup>4</sup> and A.M. Rashidi<sup>5</sup>

<sup>1</sup> Center of Excellence in Electrochemistry, School of Chemistry, College of Science, University of Tehran, Tehran, Iran.

<sup>2</sup> Catalysis Research Division, Research Institute of Petroleum Industry (RIPI), West Blvd. Azadi Sport Complex, P.O. Box 14665-137, Tehran, Iran.

<sup>3</sup> Biosensor Research Center, Endocrinology and Metabolism Molecular-Cellular Sciences Institute, Tehran University of Medical Sciences, Tehran, Iran.

<sup>4</sup> Energy Technology Research Division, Research Institute of Petroleum Industry (RIPI), West Blvd. Azadi Sport Complex, P.O. Box 14665-137, Tehran, Iran.

<sup>5</sup> Nanotechnology Research Center, Research Institute of Petroleum Industry (RIPI), West Blvd. Azadi Sport Complex, P.O. Box 14665-137, Tehran, Iran.

\*E-mail: [ganjali@ut.ac.ir](mailto:ganjali@ut.ac.ir)

*Received:* 2 February 2020 / *Accepted:* 18 March 2020 / *Published:* 10 April 2020

---

Recently, the development of highly active electrocatalysts with considerable, efficiency and moderate costs for application in the oxygen reduction reaction (ORR) has attracted a great deal of attention. In this work, an economic and easy approach has been evaluated for preparation of graphene doped with N, S, B and P. The source of graphene used in this study was grape leaves and N, S, P and B were then added thereto through a 2-hour pyrolysis reaction in N<sub>2</sub> atmosphere at 900°C. The produced specimens were evaluated using XRD, FTIR, SEM, XPS and TEM, as well as CV analyses using a rotating disk electrode (RDE). The morphology of doped graphene sample showed uniform dispersion of sulfur, nitrogen, boron and phosphorous in the carbon framework, which was obtained with elemental mapping distribution. The prepared samples show good selectivity to the 4 electron reaction pathway in an alkaline electrolyte as well as stable current density and great resistance against crossover effects of methanol. These indicate the considerable promise of these materials for use in oxygen reduction reaction as an electro-catalyst. Moreover, the onset potential of GI300G-900 and GI6-900 samples (0.93 and 0.92 V vs. RHE) was found to be near that of Pt/C 20 wt.% (0.99 V vs RHE).

---

**Keywords:** Grape leaves, Alkaline fuel cell, Graphene, Metal-free catalyst, Oxygen reduction reaction (ORR)

## 1. INTRODUCTION

Fuel cells have been used as a valuable power sources for different electric devices which platinum and its alloys applied as the most attractive electro-catalysts in them. Many researches have been focused on the applying various kinds of carbon nanostructure as the electro-catalysts. The selection criteria of new types of electro-catalysts over platinum has been focused on their advantages, including low cost and poisoning effect, and high efficiently, durability and stability [1, 2].

Among different types of carbon materials, graphene shows excellent electrical, chemical, and mechanical properties, which is suitable for ORR. In order to improvement of its electrochemical performance, heteroatoms are introduced in the graphene structure [3, 4].

Nitrogen, sulfur, boron and phosphorus as the dopants can provide the more active site of the graphene, enhance the electrical properties of catalyst and ORR performance [5-8]. Therefore, the materials containing desired heteroatoms should be selected for introducing these elements to graphene structure.

Heteroatom-doped graphene (HDG) is synthesized through "in situ" or "post-treatment" doping approaches [9, 10]. Also, many costly, yet hazardous, chemical precursors have been already used to prepare HDG, which are preferred to be replaced with less hazardous materials [11-14]. Therefore, considering this issue, a few researchers have used natural resources such as mushroom including nitrogen, which indicates biomass constitutes a source for preparing efficient electrocatalysts for ORR [15, 16].

In this regards, grape leaves (GL) that widely distributed all over the world, due to their good taste and high nutritional values are considered as a famous food. However, they included various elements like C, N, B, S, Mg, Fe and P depending on their soil cultivation which can be considered as a suitable precursor for ORR.

In this work, for the first time a new, economic and facile approach was applied for synthesis of heteroatoms-doped graphene using grape leaf as the N, S, P and B starting precursors. The heteroatoms were inserted to the graphene sheet via pyrolysis method using nitrogen atmosphere. The ORR activity of the prepared electrocatalyst was evaluated under alkaline condition. The obtained results revealed that good performance towards four-electron oxygen reduction pathway, improved onset and stability as opposed to commercially available Pt/C 20 wt.% electrocatalysts as well as environment friendly and economic cost.

## 2. EXPERIMENT

### 2.1. Materials and reagents

The grape leaves were prepared from Tehran garden in Iran. KOH, (99.8%) CH<sub>3</sub>OH, (37%) HCl, a 5 wt% solution of Nafion in ethanol/water, and Pt/C 20 wt.% (20 wt% Pt on Vulcan XC72) were obtained from Sigma-Aldrich Co.

## 2.2. Characterizations techniques

Thermo-gravimetric and differential thermo-gravimetric (TGA-DTG) tests on the dried GI powder were performed using a Perkin Elmer Pyris 1 differential analyzer under N<sub>2</sub> flow. The X-ray diffraction pattern was obtained using a Kemat DX-27 device using CuK<sub>α</sub> (k = 0.154 nm) radiation. The patterns were recorded between 10 to 80°. The morphology evaluations were conducted using a Mira-TSCAN Field emission scanning electron microscope and an acceleration voltage of 5.0 kV was applied in EDS mapping studies. FTIR spectra were obtained by a Bruker spectrometer (IFS-88) with 4 cm<sup>-1</sup> resolutions. A micromeritics Tristar 3000 instrument at 77 K was applied to nitrogen adsorption/desorption experiments. Prior to the experiments, samples were degassed at 373K for 4 hours. Raman studies were conducted on an Almega Thermo Nicolet, using an Ar ion laser with an excitation wavelength of 514 nm. The surface chemistry and bonding states of the samples were evaluated through X-ray photoelectron spectroscopy (XPS) experiments on a 5700 XPS instrument, using Al K<sub>α</sub> as the exciting source (1486.6 eV photons) operated at 350 W to identify the bonding state surface and chemical composition. Multipak<sup>TM</sup> software package was used for data processing and a Shirley background subtraction routine was applied throughout. Transmission electron microscopy (TEM) analyses were performed at 100 kV using a Hitachi-600 electron microscope.

## 2.3. Synthesis of samples

A metal oxide catalyst was used to prepare porous graphene (PG) through chemical vapor deposition (CVD) at 900-1050°C. The preparation reaction was 2-50 min. The carbon feed was methane gas which was used at a 4:1 ratio with the carrier gas. Synthesized porous graphene was purified using HCl 18% for 3 h at 30°C, washed with deionized water until pH=7, and dried at 100 °C [17, 18]. Graphene support is used as conductive support.

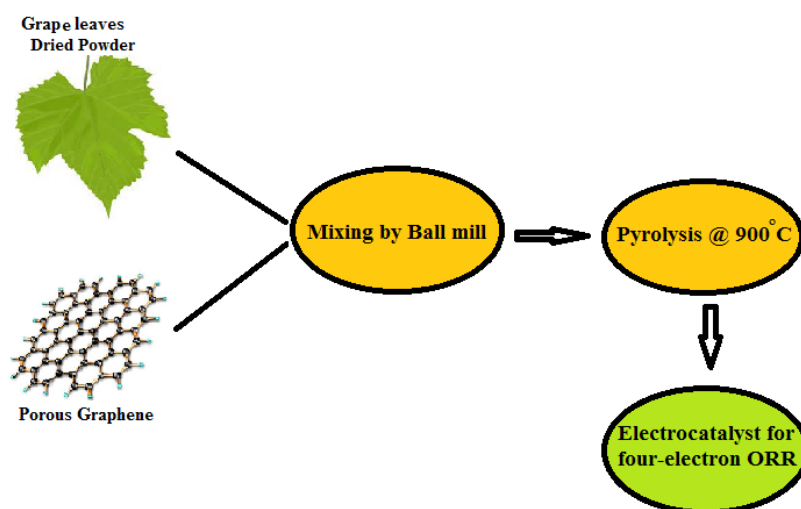


**Figure 1.** Schematic diagram of GIg-900 synthesis from Grape leaves and Porous graphene support

The fresh Grape leaves (Gl) was dried in a vacuum-drier at 60 °C, then ground prior to use the source of heteroatoms. A 1:2 wt% mixture of graphene and homogeneous Gl powders was prepared, and ground using a ball-mill for 1 h at 300 rpm. The resulting mixture was next pyrolyzed a tubular furnace with an N<sub>2</sub> atmosphere at 900°C for 2h to obtain a heteroatom-doped graphene sample (GIG-900). The tubular furnace was controlled with a program. The described procedure is schematically illustrated in Figure 1.

In addition, the thermo-gravimetric analysis (TGA-DTA) of dried Gl powder was used to determine the carbonization temperature of Gl, which indicated in Figure 2. TG measurements were recorded in N<sub>2</sub> atmosphere, in the range of 100 to 700 °C at a 10 °C/min rate.

According to the TGA-DTA results, the decomposition of Gl structure was occurred at approximately 300°C. For preparing another sample, Gl was carbonized to 300°C at 10°C/min under nitrogen condition and maintained for 5 h for the reaction to complete.

Next, a 2:1 wt.% mixture of carbonized Gl and graphene was prepared and ball milled for 60 minutes at 300 rpm. This mixture was next thermally treated (pyrolyzed) at 900°C for 2h in an N<sub>2</sub> atmosphere. The synthesized sample was labeled as Gl300G-900. To check the synergetic effect of inserting heteroatom from Gl to Graphene structure, dried Gl powder was directly pyrolyzed under similar conditions (Gl-900).

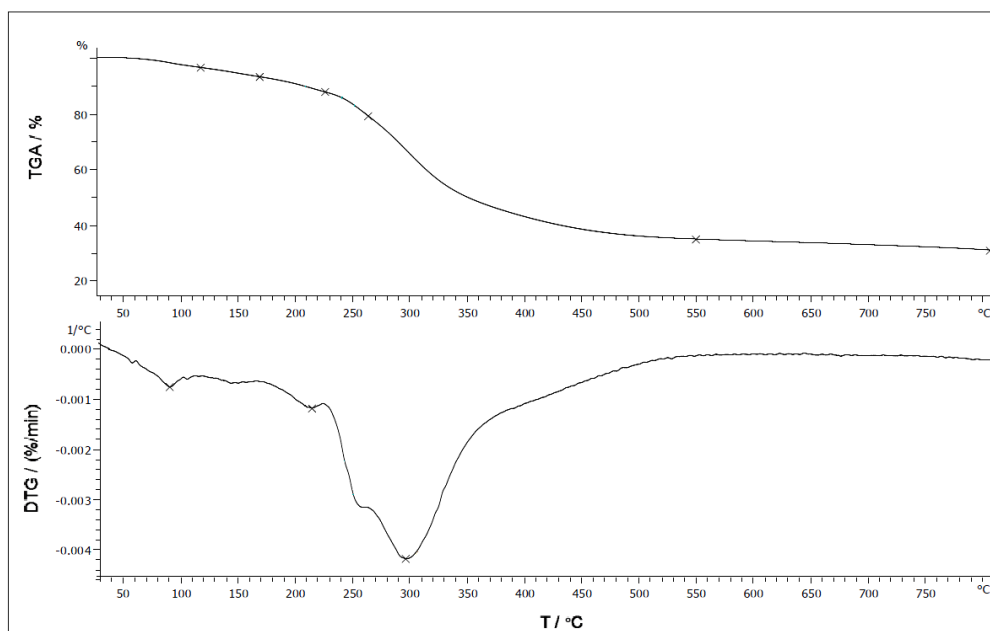


**Figure 2.** The Thermo-gravimetric and differential thermo-gravimetric (TG-DTG) analysis of Grape leaves (Gl) dried powder

#### 2.4. Electrochemical evaluations

Using an Autolab PGSTAT30 potentiostat/galvanostat workstation including three electrodes in room temperature was applied for the electrochemical measurements. A Pt wire counter electrode and an Ag/AgCl reference electrode were used in the electrochemical setup.

Each sample was sonicated in ethanol and diluted nafion solution for 30 minute and prepared a suspension in 5 mg mL<sup>-1</sup>. Then, the electrocatalyst was loaded onto a glassy carbon electrode (GCE) to reach a loading of 0.3 mg cm<sup>-2</sup>, and dried in air at 60°C. The resulting electrode was used as a working electrode. The Platinum electrocatalyst was also deposited with the same procedure.

To determine the electrocatalytic activity of the samples (loaded on the RDE) in ORR an oxygen-saturated 0.1 M solution of KOH was subjected to linear sweep voltammetry (LSV) regimes at 5 mV s<sup>-1</sup> in the potential window of -1 to 0.2 V at RDE rotations of 250, 500, 750, 1000, 1250, 1500, 2000, 2500, 3000 and 3500 rpm. The electron transfer behavior was evaluated using the Koutecky–Levich equation [19, 20].

$$\frac{1}{j} = \frac{1}{j_k} + \frac{1}{j_d} = \frac{1}{j_k} + \frac{1}{B \omega^{1/2}}$$

$$j_d = 0.62 n \times F \times (C_0) \times (D_0)^{2/3} \times (A)^{-1/6} = B \omega^{1/2}$$

$$B = 0.62 n \times F \times (C_0) \times (D_0)^{2/3} \times (A)^{-1/6}$$

In this equation J expresses the experimental current density, J<sub>L</sub> is the diffusion limiting current density and J<sub>K</sub> expresses and the kinetic limiting current density. F is 96485 C/mol (Faraday constant); n is the number of transferred electrons and ω is the rotation speed of the RDE in rpm. Further the respective values of bulk concentration and diffusion coefficient of O<sub>2</sub>(D<sub>0</sub>) in 0.1 M KOH and the and kinetic viscosity (ν) values are C<sub>0</sub>=1.2×10<sup>-6</sup> mol/cm<sup>3</sup>, D<sub>0</sub>=1.9×10<sup>-5</sup> cm<sup>2</sup>/s and 0.01 cm<sup>2</sup>/s, respectively.

Cyclic voltammetry (CV) tests were also performed at 50 mV/s in the voltage window of 0.2 V to -1.0 V (vs. Ag/AgCl).

### 3. RESULTS AND DISCUSSION

#### 3.1. Structural Characterization

Changes in the structure of the carbon material due to doping were evaluated based on the XRD patterns. Figure 3 shows XRD pattern of PG, GI-900 and GI300G-900 samples in 2θ range from 10 to 80°. In Figure 3-a, the peaks in 2θ equal 25.1° and 42.8 are indicative of the (002) and (100) graphite structure reflection and formation of porous graphene, respectively [17, 18, 21]. High-temperature pyrolyzed GI-900 sample Figure 3-b showed peaks at 2θ= 21 and 44.9, which are indicative of graphitized carbon materials. Moreover, the peak approximately ~25.9 and 42.8, were attributed to 002 and 100 lattice planes of graphitic crystal structure. This indicates that this structure is not damaged in GI300G-900 [16, 22].

Also, the peak at (002) attributed to the carbon peak of GI300G-900 underwent a positive shift toward higher 2θ values (25.9), as opposed to porous graphene (25.1), as a result of the slight distortion in crystalline structure along (a) or (b) directions, as a result of the incorporation of heteroatoms in the sp<sup>2</sup> carbon network, and proliferation of defects in the sheets. These reflect the modification of PG with N, S, B, and P-rich fragments of thermally decomposed GI [16]. From the XRD data, the interlayer

distances (d-spacing) of the carbon nano-sheets in G1300G-900 sample was determined to be smaller than that of for PG with a higher disorder degree. This change is due to heat treatment effect under high temperature at 900 °C which leads to decrease in the interlayer spacing [23]. In the case of peak 002 of PG the full width-half maximum (FWHM) was smaller than that of for G1300G-900, which originates from the increase in the grain size, and also due to the introduction of heteroatoms in the carbon framework.

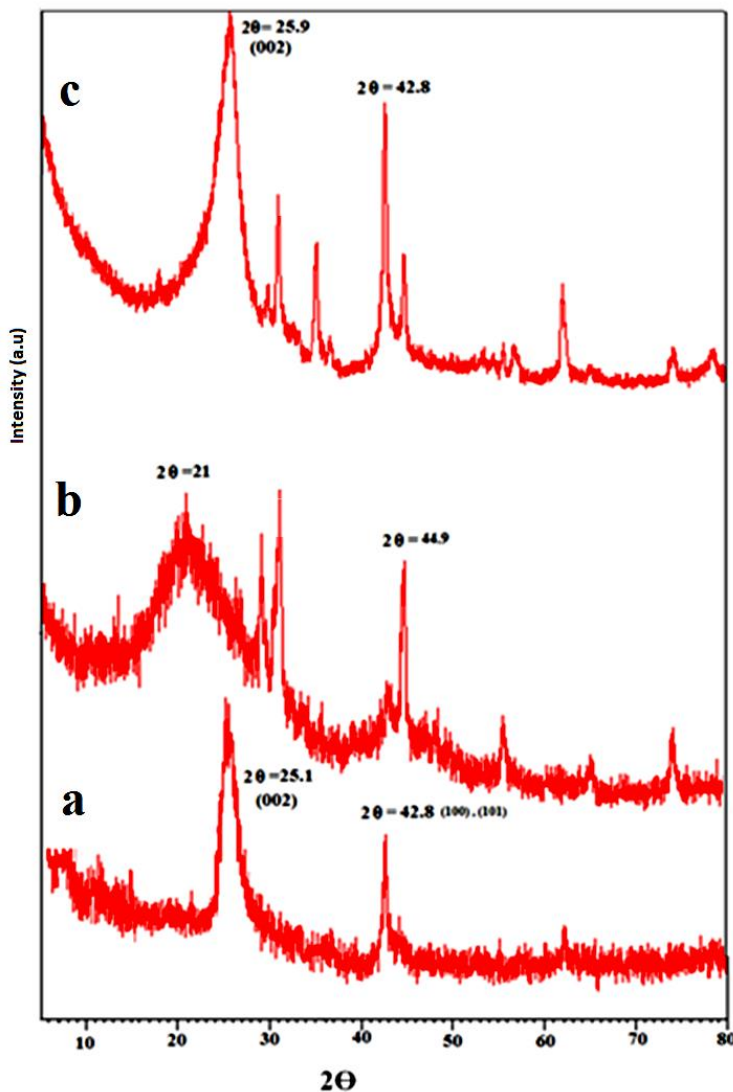


**Figure 3.** XRD pattern of a: PG, b: G1-900 and c: G1300G-900

Also, heteroatoms doping level in graphene structure and defects were investigated using Raman spectroscopy. The G, D, and 2D peaks respectively at  $\sim 1580$ ,  $\sim 1350$  and  $\sim 2680$   $\text{cm}^{-1}$  in the Raman spectrum are three important peaks characteristics of graphene structure. The former corresponds to the vibrations of the  $\text{sp}^2$  carbons, whereas the D band indicates the incorporation of heteroatoms in the network of carbon atoms and the corresponding disorder in the  $\text{sp}^2$  carbon atoms or defects [24, 25].

The ratio of the intensities of D and G bands ( $I_D/I_G$ ), shows carbon structure disordering. The higher value of  $I_D/I_G$  is indicative of increases in the number of defects in the structure of graphene and

the presence of heteroatoms. The Raman result shows that the GI precursor used as heteroatom dopant simultaneously enable to enter heteroatoms into the graphene sheets which could affect  $I_D/I_G$  ratio (Figure 4).

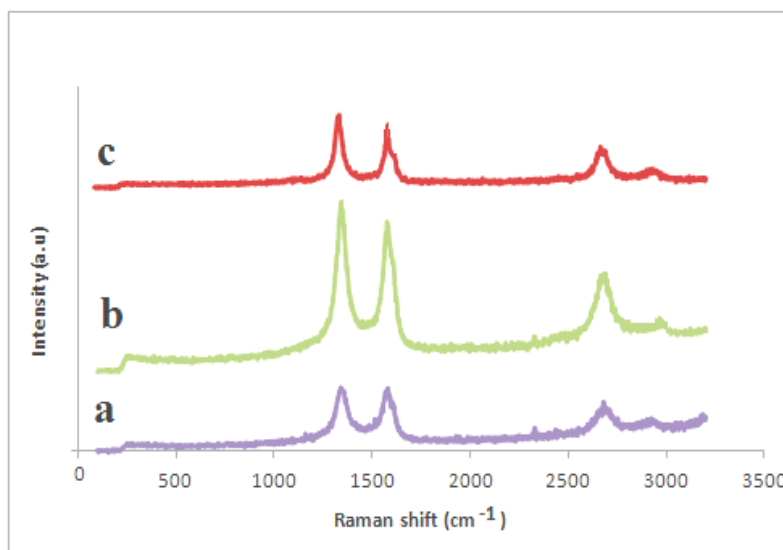


**Figure 4.** Raman spectra of (a) PG, (b) GI300G-900, (c) GI900

**Table 1.** Raman specification of normal and co-doped PG

Sample	G band (cm <sup>-1</sup> )	D band (cm <sup>-1</sup> )	2D band (cm <sup>-1</sup> )	$I_D/I_G$
PG	1577.2	1341.85	2681.17	0.96
GI900	1581.76	1341.603	2681.17	1.13
GI300G-900	1577.12	1343.99	2679.13	1.17

Table 1 indicates the  $I_D/I_G$  values for PG, GI300G-900 and GI900 samples which are calculated to be 0.96, 1.17 and 1.13 respectively. The  $I_D/I_G$  value of heteroatoms doped catalysts, GI900 and GI300G-900 samples, were higher than that of for PG (0.96), indicating more defects and disordered structures as well as a low degree of graphitization, that cause improving the adsorption and oxygen diffusion, as well [26-39]. D + G combination peak at about 2950 cm<sup>-1</sup> in the Raman feature (Figure 3) is induced by the defects. The peak at 2400 cm<sup>-1</sup> is associated to the N<sub>2</sub> gas present in the air surrounding the sample [30].

The functional groups in graphene structure and heteroatom doped-Graphene was investigated using Fourier transform infrared (FTIR) spectroscopy. Typical FTIR spectra of PG, G1-900 and G1300G-900 can be seen in Figure 5. The peaks at approximately 3400, 1032, 1571 and 1725  $\text{cm}^{-1}$  in the case of PG clearly indicate the presence of adsorbed water molecules, as well as stretching of C-O, C=C and C=O (carbonyl) groups.

In the G1300G-900 prepared sample, the peaks appeared at 1652, 1597, 1505, 1498 and 1187  $\text{cm}^{-1}$  correspond to the strong and sharp peak C=N, N=O, N=O, N-O and C-N bonds, respectively. Besides, appearance of two peaks approximately 700 and 1108  $\text{cm}^{-1}$  correspond to the vibrations of C-S and C=S bonds. However, the band reflecting that of C-O either greatly lost their intensity or fully disappeared [31, 32]. Moreover, the bands at 1038, 1100 and 600  $\text{cm}^{-1}$  corresponds to P=O, B-C and B-N, respectively. In the case of G1-900, the signals of the double bonds in C=O, C=N, N=O, N=O, S=O, P=O and C=S appeared at 1795, 1652, 1598, 1505, 1413, 1038 and 1108  $\text{cm}^{-1}$ , respectively. In addition, peaks at 1498, 1044, 700 and 600  $\text{cm}^{-1}$  reflect the vibrations of N-O, C-N, C-S and B-N [33].

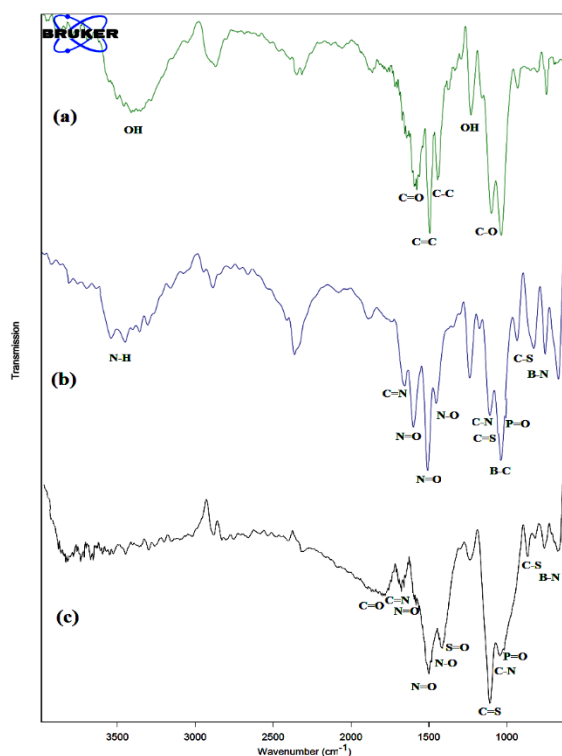


**Figure 5.** FTIR spectra for PG and as-synthesized doped samples; PG (a), G1300G-900 (b) and G1-900(c)

Figure 6-a shows adsorption-desorption isotherms of PG and doped samples including G1G-900 and G1300G-900. According to the IUPAC classification, the isotherms represent a typical curve (type IV) along with a hysteresis loop initiating at an approximate relative pressure of 0.4 implies that graphene contains slit-shaped mesopores [34].

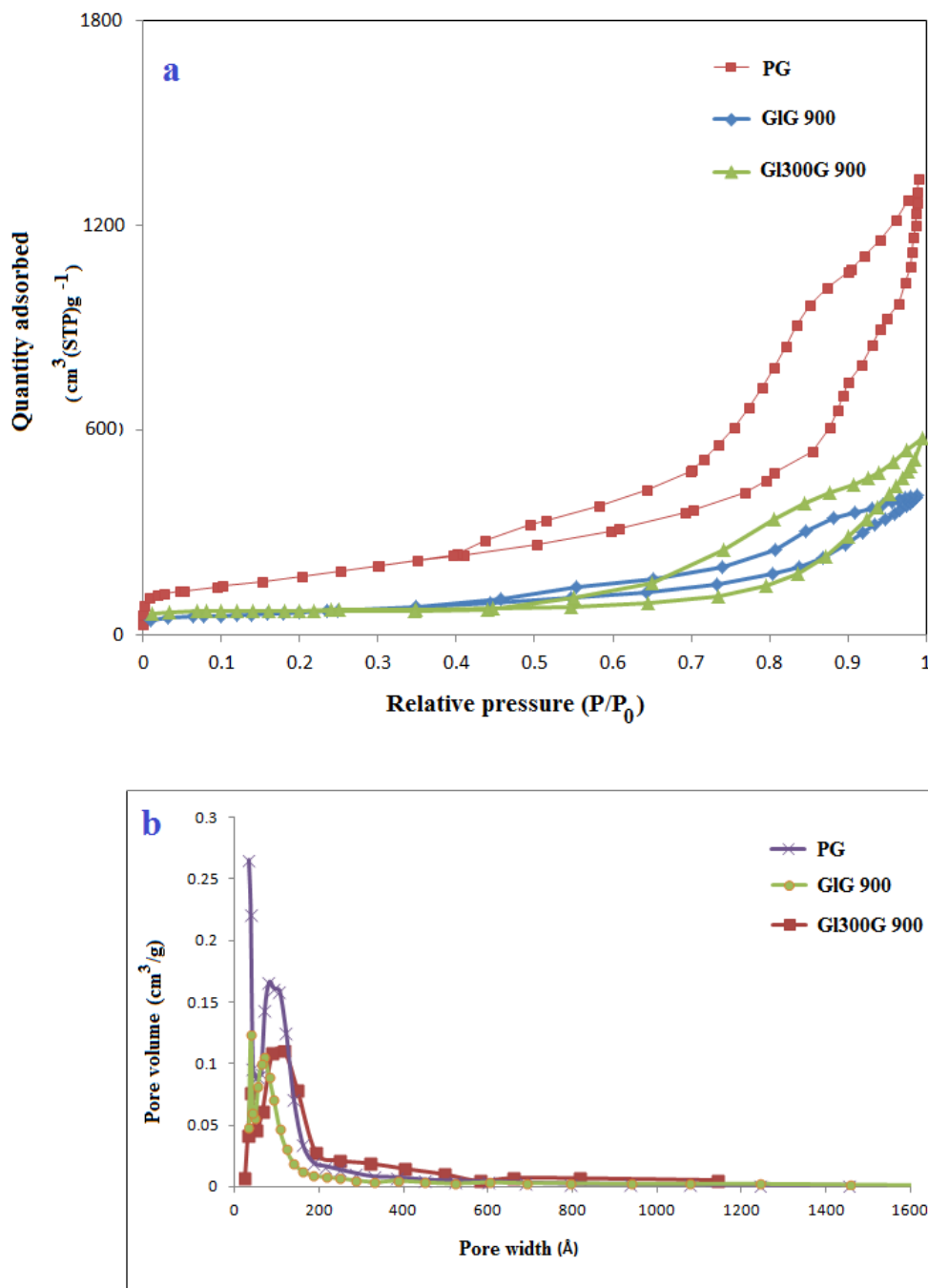


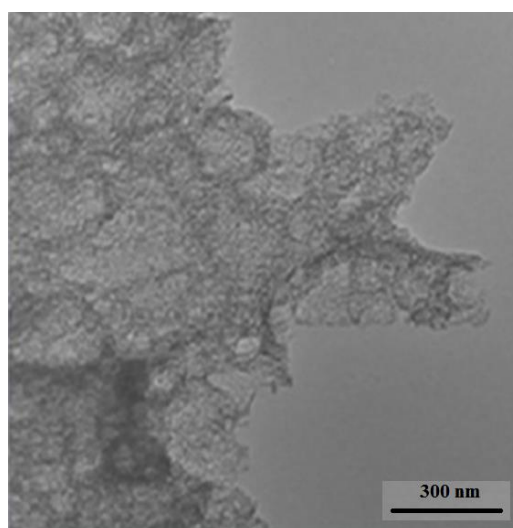
**Figure 6.**  $N_2$  adsorption isotherms of pure and heteroatoms-doped PG (a), Pore size distribution of samples (b)

Moreover, average pore size distribution values for the samples have been illustrated in Figure 6-b. Also, the textural properties including the values of BET specific surface area, pore volume and diameter of PG, GIG-900 and GI300G-900 are shown in Table 2.

**Table 2.** Textural parameters of pure and heteroatoms-doped PG

Sample	BET Surface Area ( $\text{m}^2\text{g}^{-1}$ )	Pore Volume ( $\text{cm}^3\text{g}^{-1}$ )	Mean Pore Size (nm)
PG	629.29	2.03	12.9
G1300G-900	243.36	0.8	12.5
G1G-900	239.34	0.6	10.1

Transmission electron microscopy image of porous graphene is shown in Figure 7, which indicates a porous structure with average pore size below 20 nm.

**Figure 7.** TEM images of PG

Furthermore, the surface morphology and EDX mapping of G1-900 and synthesized doped graphene (Figure 8) were studied by FESEM. It can be seen that the morphology of the sample is comparable to graphene base. The elemental mapping distribution proves the presence of nitrogen, sulfur, boron and phosphorous in the pyrolyzed grape leaves sample. Moreover, uniform dispersion of these elements is observed in the carbon structure, which reflects the successful incorporation of heteroatoms in the PG structure.

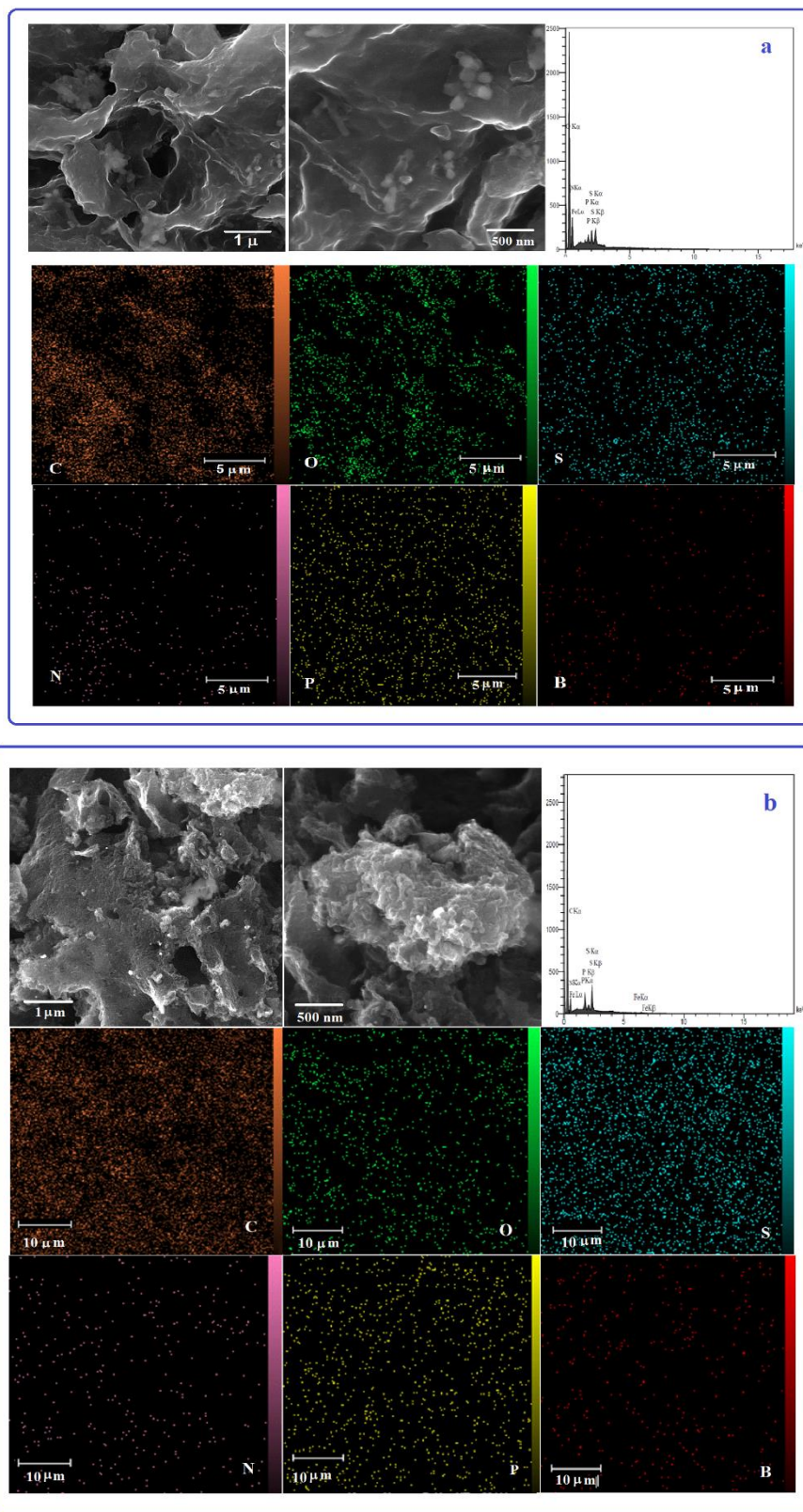


**Figure 8.** FESEM micrographs of prepared samples in two magnification levels and EDX mapping of C, O, S, N, P and B in (a) the GI-900, (b) the GI300G-900 samples

Through X-ray photoelectron spectroscopy the chemical bonding of GI300G-900 was assessed. Figure 9 illustrates the XPS spectrum obtained over a wide energy range of 0-1400 eV. This spectrum

mainly contains a narrow graphitic C 1s peak at ~284.4 eV. Apart from this predominant peak N 1s, S 2p, P 2p and B 1s peaks at ~400 eV, ~165 eV, ~133 eV and ~190 eV, respectively. Also, an O 1s peak at ~530 eV for adsorbed oxygen, reflecting the physical incorporation of O in the PG framework.

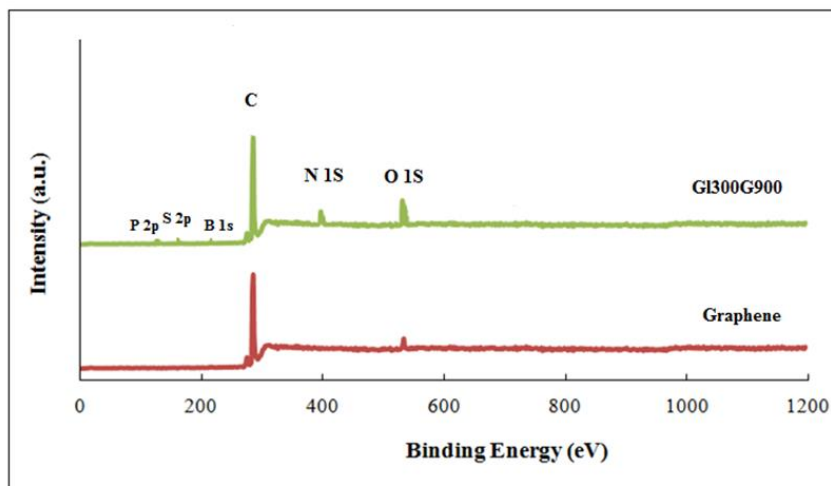


**Figure 9.** XPS of pure and as-synthesized GI300G-900 PG

The high-resolution XPS (HR-XPS) C1s peak Figure 10a could be deconvoluted into three corresponding peaks at approximately 284.6, 285.9 and 288.0 eV, correspond to the C=C, C–N or C–C and O–C=O bonds. In addition, the high-resolution XPS spectra for all the doped elements in GI300G900 sample are shown in Figure 10 (a-e).

From the high resolution spectrum, a strong S 2p peak Figure 10-b shows significant amount of S doped atoms. Besides, the deconvolution analysis shows the peak approximately 163.8, 165.0 and 168.8 of the S 2p reflect the presence of C=S, sulfoxide and other oxidized forms [35].

The HR-XPS N 1s spectra of the doped PG with a nominal nitrogen level of 2 % (Table 3) from the spectra collected at different locations can be resolved into three main peaks Figure 10-c, of pyridinic N at 398.9 eV, nitrogen in the N–B–C configuration at 399.8 eV, and pyridinic N-oxide at 402.5 eV [27, 29, 35-38].

The binding energy of B1s at approximately 193 eV Figure 10-d is attributed to the boron oxide. However, the binding energy of approximately 191 eV, indicates the successful incorporation of B atoms in the PG framework. The deconvolution of high resolution B1s XSP result shows three sub-peaks, attributed to B-C (191.1 eV), B-C-N (189.2 eV), and B-O (193 eV) bonds [36].

The HR-XPS results reflects covalent binding of B and N graphene carbons. These atoms are also partially covalently bond (B–N bond) with each other according to peak at approximately 189.2 eV. The P 2p XPS spectra of GI300G-900 Figure 10-e indicates the P-O and P-C binding energy peaks at 133.6 eV and 132.6 eV, respectively; confirms the P-doping feature [39]. The XPS results of elements concentration, chemical state and peaks position in GI300G-900 is shown in Table 3.

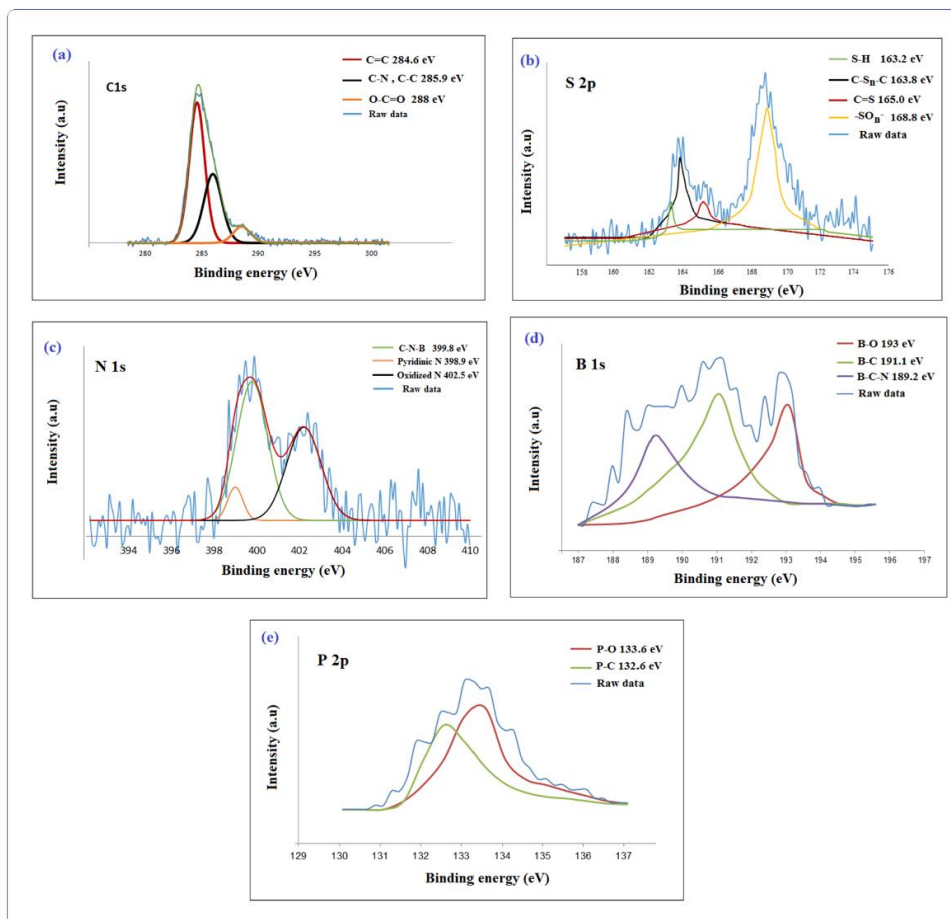


**Figure 10.** The HR-XPS spectra of GI300G-900, (a) C 1s, (b) S 2p, (c) N 1s, (d) B 1s, (e) P 2p

**Table 3.** The XPS results of elements concentration, peaks position and their percent in GI300G-900 sample

Sample	Element	At. Concentration, %	Binding Energy, eV	%
GI300G-900	C	88.8	284.6	72.8
			285.9	12.0
			288	4.0
	N	2.0	398.2	0.2
			399.8	1.0
			402.5	0.8
	S	1.5	163.2	0.1
			163.67	0.5
			165.00	0.2
			168.53	0.7
	B	1.2	191.1	0.5
			193	0.36
			189.2	0.34
	P	0.7	133.6	0.45
132.6			0.25	
O	5.8			

According to these results, nitrogen, sulfur, phosphorus and boron incorporation to graphene structure were verified by XPS data. Therefore, these elements have been successfully doped in graphene structure and heteroatoms could bond to carbon using high temperature pyrolysis method [25, 40].

### 3.2. Electrochemical Evaluation

#### 3.2.1. Cyclic voltammograms (CVs) results

The behavior of GI300G-900 and GI900 as electrocatalysts was investigated through cyclic voltammetry tests in an O<sub>2</sub> saturated 0.1 M KOH solution [41-43]. The results were further compared with those of PG and Pt/C 20 wt.% samples, which is represented in Figure 11.

Based on the results, using a PG electrode ORR could be observed after 20 reducing CV cycles at 0.82 V (vs RHE) with the cathodic oxygen reduction peak at approximately 0.73 V (vs RHE). All the prepared doped graphene samples had positive onset potentials and stronger ORR reduction peaks as opposed to undoped PG. Moreover, the peak current densities of the doped samples were also higher, indicating that co-doping of N, S, B and P atoms into graphene improves its electro catalytic-activity in ORR.

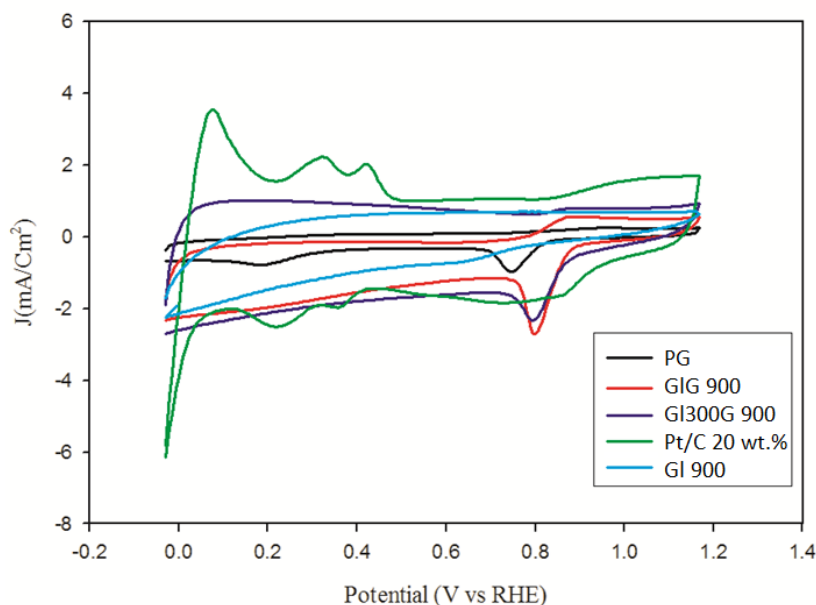


**Figure 11.** CVs of the doped samples in an O<sub>2</sub> saturated 0.1 M KOH at 50 mV/s for PG, Pt/C 20 wt.%, GI900 and GI300G 900 loaded electrodes.

#### 3.2.2. Tests with loaded Rotating Disk Electrodes (RDEs)

The performance and kinetic behavior of the prepared samples as ORR electrocatalysts were further investigated by loading them on an RDE and performing tests at 250 to 3500 rpm. Moreover, the electrons number involved in the electrocatalytic reaction was calculated using the Koutechy–Levich equation [21, 41, 43]. Plots of  $-J^{-1}$  against  $\omega^{-0.5}$  plots were drawn based on data obtained at potentials in the range of 0.45 to 0.65 V (vs RHE) and are presented in Figure 12 and table 4. Based on these results

the ORR occurs through two 2- and 4-electron mechanisms based on the nature of the samples. GI300G 900 was observed to selectively host the 4-electron mechanism in alkaline media.

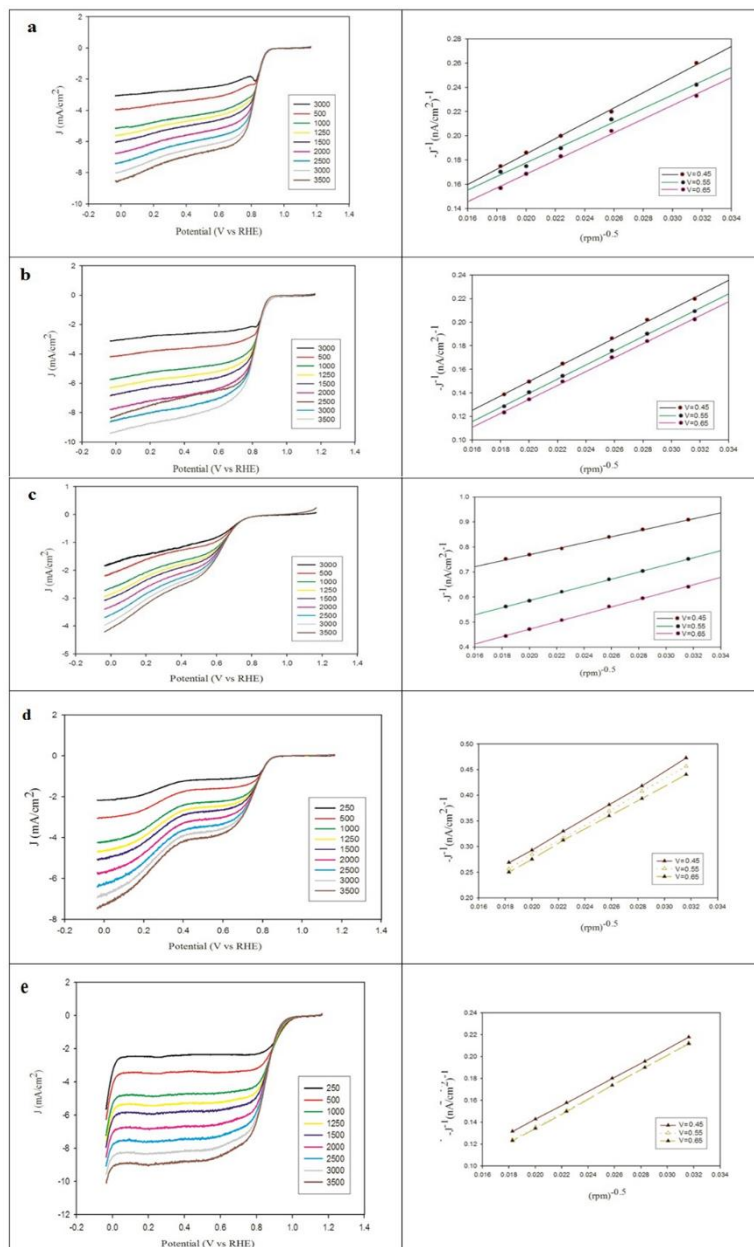


**Figure 12.** Linear sweep voltammetry at 5 mV/sec and various rotation rates in KOH 0.1 M, and the analogous Koutecky–Levich plots at different potentials for: GIG-900 (a), GI300G-900 (b), GI-900 (c), PG (d) and Pt/C 20 wt.% (e)

Figure 13 represents the LSV curves for all prepared electrocatalysts, recorded in an O<sub>2</sub>-saturated 0.1 M solution of KOH at 5mv/sec and a rotation rate of 1500. The results have also been compared with those of PG and Pt/C 20 wt.% in this figure.

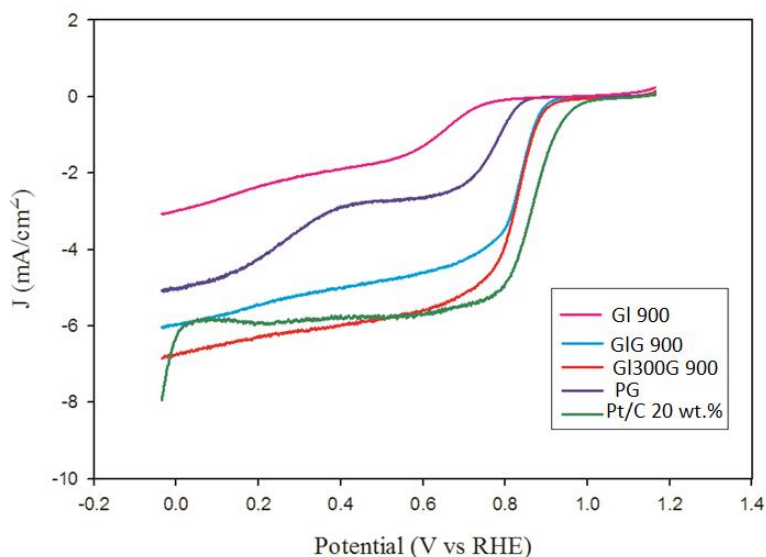


**Figure 13.** LSV plots of the different electrocatalysts at 1500 rpm in an O<sub>2</sub>-saturated 0.1 M solution of KOH.

According to this figure, the ORR of the PG electrode commenced at approximately 0.85 V (onset potential), while the ORR onset potential of the GI300G-900 and GIG-900 electrodes were approximately 0.93 and 0.92 V, which are higher than porous graphene. These observations suggest that the presence of N, S, P, and B atoms increases the number of active sites and gives rise to more efficient ORR through a 4-electron pathway.

The values of the onset potential, number of transferred electrons and current density of the prepared electrocatalysts and Pt/C 20 wt.% are presented in Table 3, for comparison.

**Table 4.** Values of the ORR onset potentials, number of transferred electrons and current density for the prepared electrocatalysts and Pt/C 20 wt.%

Samples	Number of electron transfer (n)	Onset potential (V vs RHE)	Steady state current density (mA/cm <sup>2</sup> )
GI-900	2.1	0.75	-3.02
GI300G-900	4.0	0.93	-6.81
GIG-900	3.3	0.92	-6.02
PG	2.2	0.85	-5.07
Pt/C 20 wt.%	4.0	0.99	-5.88

The electron transfer number of GI-900, GIG-900 and GI300G-900 samples in ORR process at potential range from 0.65 to 0.45 was 1.9-2.3, 3.2-3.4 and 3.9-4.1 respectively. The ORR onset and current steady state of the GI-900 and GI300G-900 and GIG-900 are shown in Table 4. GI300G900 has a similar behavior to Pt/C 20 wt.%, and undergoes a 4e<sup>-</sup> ORR.

3.2.3. Methanol stability experiments

Furthermore, the stability of the electro-catalyst loaded electrodes and CH<sub>3</sub>OH crossover of the electrocatalysts were investigated before and after methanol addition (1M) during the chronoamperometry analysis [21, 41, 43]. The plots of current density of the doped graphene samples (GIG-900 and GI300G-900), PG, GI-900 and Pt/C 20 wt.% against time, recorded in an O<sub>2</sub>-saturated 0.1 M solution of KOH electrolyte, at a kinetic-controlled potential of 0.86V at 5000 s.

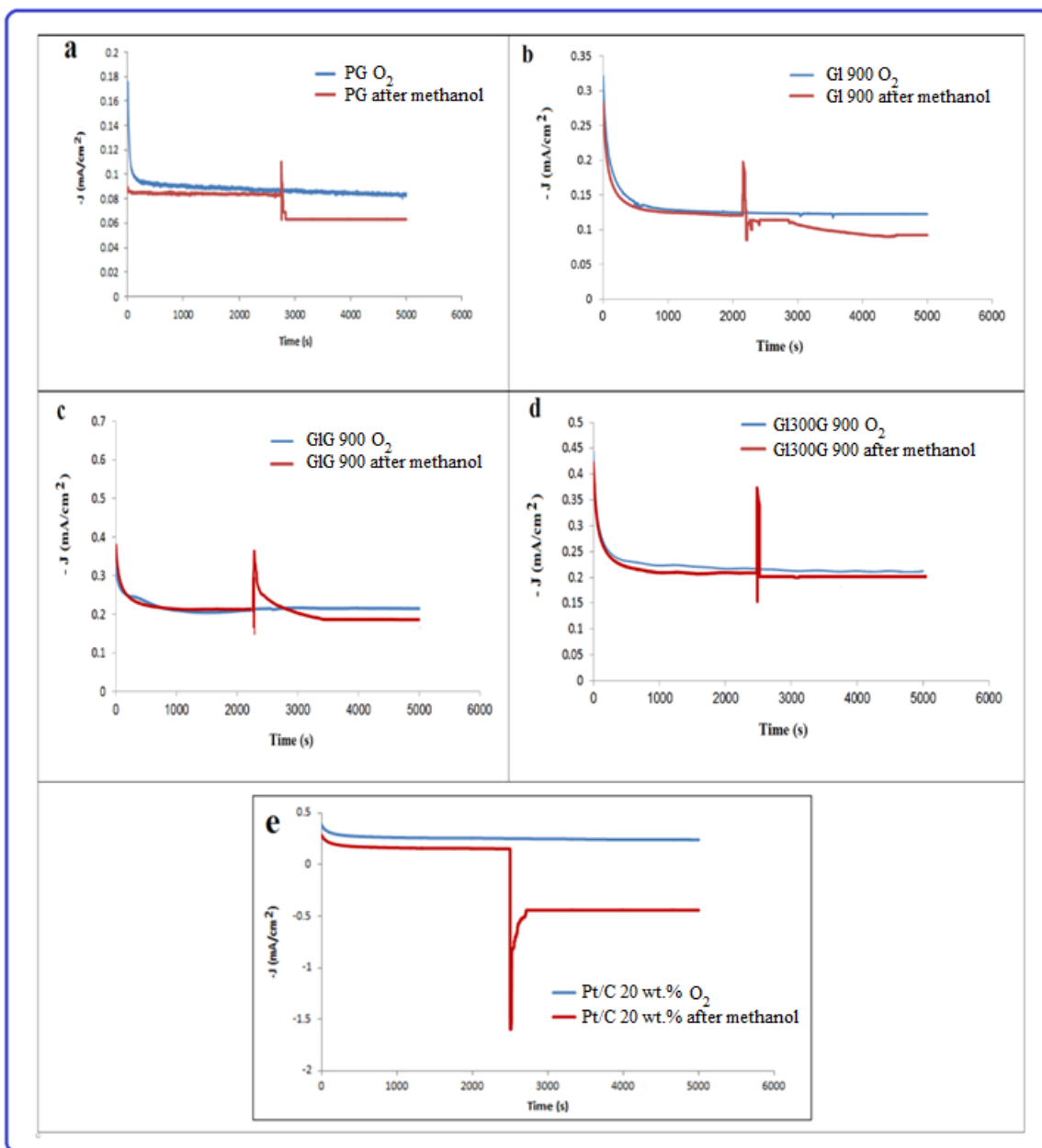


**Figure 14.** Current density-time plots for (a) PG, (b) GI 900 (c) GIG-900 (d) GI300G-900 and (e) Pt/C 20 wt.% electrodes in O<sub>2</sub> saturated 0.1 M KOH in presence of methanol

As the results demonstrate, the GI300G-900 and GIG-900 electrocatalysts show better stability of the current density and CH<sub>3</sub>OH tolerance after 5000s, as compared with PG and Pt/C 20 wt.%. The

results indicate long-term stability in the case of the co-doped graphene electrocatalysts. This can be attributed to the presence of active heteroatoms, such as pyridinic and oxidized N in the graphene framework, which enhance the electrical conductivity and catalytic activity.

In addition, toward  $\text{CH}_3\text{OH}$  crossover tolerance of the synthesized samples and stability of the electrodes were studied before and after methanol addition (1M) during the CV measurements.

As Figure 15 shows, after adding methanol the peak corresponding to the reduction of oxygen by PG and Pt/C 20 wt.% diminished and disappeared, respectively. However, CV measurements showed the unchanged and stable oxygen reduction peak after several CV cycles for the prepared doped samples after methanol addition, indicates the outstanding  $\text{CH}_3\text{OH}$  crossover tolerance to the in the case of the doped graphene electrocatalysts.

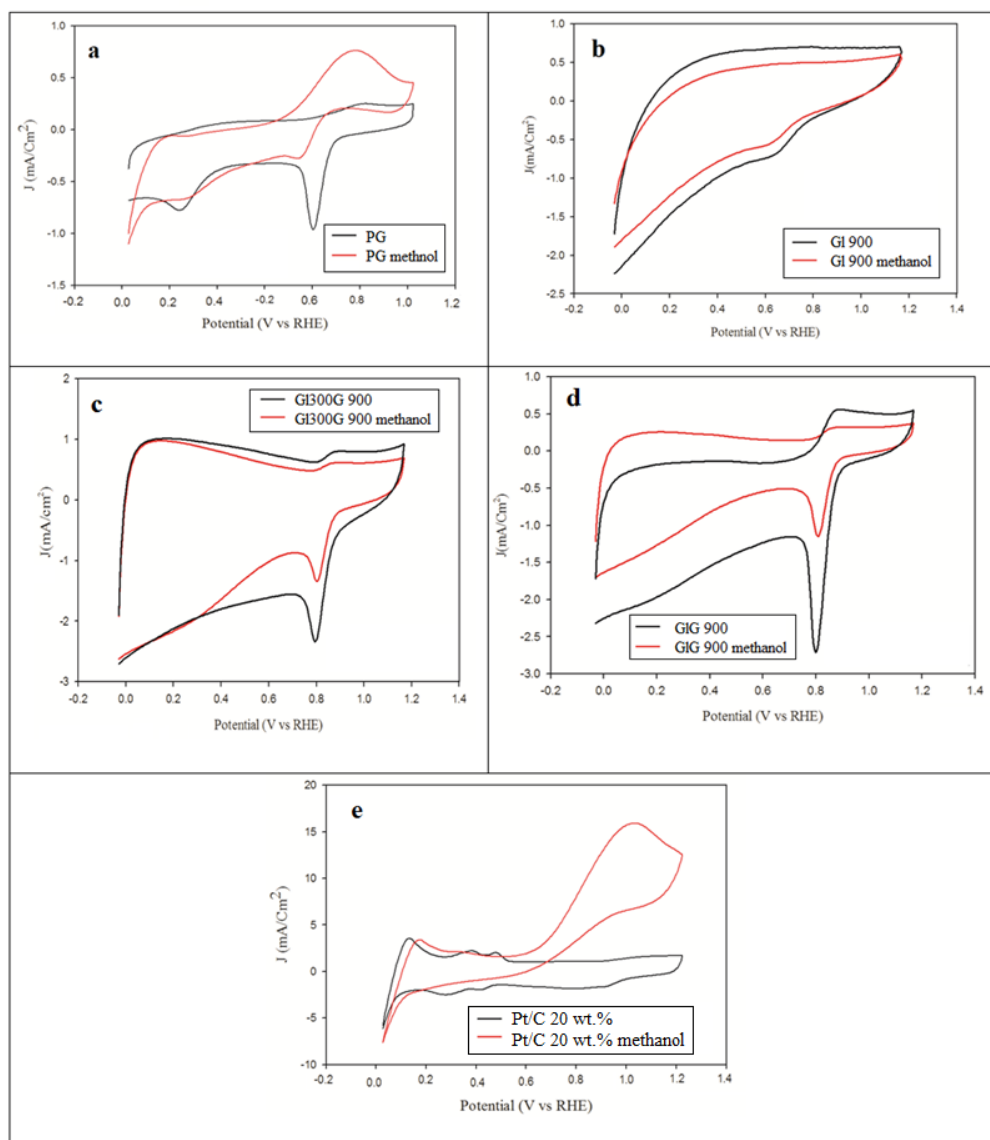


**Figure 15.** Cyclic voltammetry of (a)PG, (b) GI-900, (c) GI300G-900, (d) GIG-900and (e) Pt/C 20 wt.% in KOH 0.1 M (scan rate: 50 mV/sec)before and after methanol addition.

#### 4. CONCLUSION

The work described the preparation and characterization of heteroatoms-doped PG samples using grape leaves. The prepared electrocatalysts, GI300G-900 and GI9-900, had enhanced stability and CH<sub>3</sub>OH crossover tolerance in comparison to PG and Pt/C 20 wt.%, with respective ORR onset potentials and number of transferred electrons of 0.93 vs RHE and 4.0; and 0.92 vs RHE and 3.3, respectively. The electrochemical performance of the heteroatom co-doped graphene catalyst (i.e., GI300G-900) represented the highly homogeneity of N, S, P and B dispersion in graphene structure, as well as an ORR behavior comparable to Pt/C 20 wt.%. The ORR onset potential of optimized catalyst 0.93 V (vs RHE) which is near that of Pt/C 20 wt.% (i.e. 0.99 V vs RHE). Moreover, these electrocatalysts conduct alkaline ORR process in 4e<sup>-</sup> electron transfer pathway. Therefore, the optimal synthesized sample "GI300G-900" prepared with grape leaves is a good and economic candidate for scale up and use in the ORR of low-temperature fuel cells and replace costly metal-based electrocatalysts, due to its low cost, good performance.

#### ACKNOWLEDGEMENTS

The authors thank the Research Council of University of Tehran and the Research Institute of Petroleum Industry (RIPI) for their financial support.

#### References

1. N. Alexeyeva, E. Shulga, V. Kisand, I. Kink, and K. Tammeveski, *Journal of Electroanalytical Chemistry*, 648 (2010) 169.
2. H. Zhang, Y. Wang, D. Wang, Y. Li, X. Liu, P. Liu, H. Yang, T. An, Z. Tang, and H. Zhao, *Small*, 10 (2014) 3371.
3. M. Park, T. Lee, and B.S. Kim, *Nanoscale*, 5 (2013) 12255.
4. G.L. Tian, M.Q. Zhao, D. Yu, X.Y. Kong, J.Q. Huang, Q. Zhang, and F. Wei, *Small*, 10 (2014) 2251.
5. H. Fei, R. Ye, G. Ye, Y. Gong, Z. Peng, X. Fan, E.L.G. Samuel, P.M. Ajayan, and J.M. Tour, *ACS Nano*, 8 (2014) 10837.
6. J.C. Li, S.Y. Zhao, P.X. Hou, R.P. Fang, C. Liu, J. Liang, J. Luan, X.Y. Shan, and H.M. Cheng, *Nanoscale*, 7 (2015) 19201.
7. M. Li, L. Zhang, Q. Xu, J. Niu, and Z. Xia, *Journal of Catalysis*, 314 (2014) 66.
8. H.Y. Park, T.J. Shin, H.I. Joh, J.H. Jang, D. Ahn, and S.J. Yoo, *Electrochemistry Communications*, 41 (2014) 35.
9. L. Chen, Z. Chen, Z. Huang, Z. Huang, Y. Wang, H. Li, H. Zhou, and Y. Kuang, *J. Phys. Chem. C.*, 119 (2015) 28757.
10. C.V. Rao, C.R. Cabrera, and Y. Ishikawa, *J. Phys. Chem. Lett.*, 1 (2010) 2622.
11. D.W. Wang, and D. Su, *Energy & Environmental Science*, 7 (2014) 576.
12. G. Wu, K.L. More, C.M. Johnston, and P. Zelenay, *Science*, 332 (2011) 443.
13. P. Chen, T.Y. Xiao, Y.H. Qian, S.S. Li, and S.H. Yu, *Adv. Mater.*, 25 (2013) 3192.
14. Y. Zheng, Y. Jiao, M. Jaroniec, Y. Jin, and S.Z. Qiao, *Small*, 8 (2012) 3550.
15. C. Guo, W. Liao, Z. Li, L. Sun, and C. Chen, *Nanoscale*, 7 (2015) 15990.
16. C. Guo, L. Sun, W. Liao, and Z. Li, *Materials*, 9 (2016) 1.
17. S. Pourmand, M. Abdouss, and A.M. Rashidi, *Int. J. Environ. Res.*, 9 (2015) 1269.
18. A.M. Rashidi, L. Mahmudian, and H. Dehghani, *US Patent*, 20160060123 (2016).

19. Z. Lin, G. Waller, Y. Liu, and C.P. Wong, *Nano Energy*, 2 (2013) 241.
20. L.T. Qu, Y. Liu, J.B. Baek, and L.M. Dai, *ACS Nano.*, 4 (2010) 1321.
21. S. Sadegh Hassani, M.R. Ganjali, L. Samiee, A.M. Rashidi, S. Tasharrofi, A. Yadegari, F. Shoghi, and R. Martel, *J. Nanosci. Nanotech.*, 18 (2018) 4565.
22. C.Z. Guo, C.G. Chen, and Z.L. Luo, *J. Power Sources*, 245 (2014) 841.
23. G. Jo, J. Sanetuntikul, and S. Shanmugam, *RSC Adv.*, 5 (2015) 53637.
24. G. Panomsuwan, N. Saito, and T. Ishizaki, *ACS Appl. Mater. Interfaces*, 8 (2016) 6962.
25. H. Lin, L. Chu, X. Wang, Z. Yao, F. Liu, Y. Ai, X. Zhuang, and S. Han, *New J. Chem.*, 40 (2016) 6022.
26. Z. Xing, Z. Ju, Y. Zhao, J. Wan, Y. Zhu, Y. Qiang, and Y. Qian, *Scientific Reports*, 6 (2016) 26146.
27. W. Ai, Z. Luo, J. Jiang, J. Zhu, Z. Du, Z. Fan, L. Xie, H. Zhang, W. Huang, and T. Yu, *Adv. Mater.*, 26 (2014) 6186.
28. Z. Sun, J. Masa, P. Weide, S.M. Fairclough, A.W. Robertson, P. Ebbinghaus, F.H. Warner, S.C.E. Tsang, M. Muhlerb, and W. Schuhmann, *J. Mater. Chem. A.*, 3 (2015) 15444.
29. Y. Su, Y. Zhang, X. Zhuang, S. Li, D. Wu, F. Zhang, and X. Feng, *Carbon*, 62 (2013) 296.
30. M.A. Pimenta, G. Dresselhaus, M.S. Dresselhaus, L.G. Cancado, A. Jorio, and R. Saito, *Phys. Chem. Chem. Phys.*, 9 (2007) 1276.
31. M. Praveen Kumar, T. Kesavan, G. Kalita, P. Ragupathy, T.N. Narayanan, and D.K. Pattanayak, *RSC Adv.*, 4 (2014) 38689.
32. R. Karimi Shervedani, and A. Amini, *Electrochimica Acta*, 142 (2014) 51.
33. S. Wang, L. Zhang, Z. Xia, A. Roy, D. Chang, J.B. Baek, and L. Dai, *Angew. Chem. Int. Ed.*, 51 (2012) 4209.
34. S. Brunauer, L.S. Deming, W.E. Deming, and E. Teller, *Journal of the American Chemical society*, 62 (1940) 1723.
35. C.B. Ma, Z.T. Zhu, H.X. Wang, X. Huang, X. Zhang, X. Qi, H.L. Zhang, Y. Zhu, X. Deng, Y. Peng, Y. Han, and H. Zhang, *Nanoscale*, 7 (2015) 10162.
36. S. Dou, X. Huang, Z. Ma, J. Wu, and S. Wang, *Nanotechnology*, 26 (2015) 045402.
37. X. Chen, X. Chen, X. Xu, Z. Yang, Z. Liu, L. Zhang, X. Xu, Y. Chen, and S. Huang, *nanoscale*, 6 (2014) 13740.
38. Y. Dong, H. Pang, H.B. Yang, C. Guo, J. Shao, Y. Chi, C.M. Li, and T. Yu, *Angew. Chem. Int. Ed.*, 52 (2013) 7800.
39. Y. Wang, B. Zhang, M. Xu, and X. He, *RSC Advances*, 5 (2015) 86746.
40. X. Qiao, S. Liao, C. You, and R. Chen, *Catalysts*, 5 (2015) 981.
41. S. Sadegh Hassani, M.R. Ganjali, L. Samiee, and A.M. Rashidi, *Int. J. Electrochem. Sci.*, 13 (2018) 11001.
42. S. S. Hassani, L. Samiee, E. Ghasemy, A.M. Rashidi, M.R. Ganjali, and S. Tasharrofi, *Int. J. Hydrogen Energy*, 43 (2018) 15941.
43. L. Samiee, S. Sadegh Hassani, M.R. Ganjali, and A.M. Rashidi, *Iranian J. Hydrogen & Fuel Cell*, 4 (2017) 231.